Journal of Macromolecular Science, Part A
Publication details, including instructions for authors and subscription information:
http://www.informaworld.com/smpp/title~content=t713597274

Structure-Property Relationships in Segmented Polyviologen Ionene Rotaxanes

Don Loveday[a]; Garth L. Wilkes[a]; Mukesh C. Bheda[b]; Ya. X. Shen[b]; Harry W. Gibson[b]
[a] Polymer Materials and Interfaces Laboratory Chemical Engineering Department, [b] Chemistry Department, Virginia Polytechnic Institute and State University, Blacksburg, Virginia

To cite this Article Loveday, Don , Wilkes, Garth L. , Bheda, Mukesh C. , Shen, Ya. X. and Gibson, Harry W.(1995) 'Structure-Property Relationships in Segmented Polyviologen Ionene Rotaxanes', Journal of Macromolecular Science, Part A, 32: 1, 1 — 27
To link to this Article: DOI: 10.1080/10601329508011061
URL: http://dx.doi.org/10.1080/10601329508011061

J.M.S.—PURE APPL. CHEM., A32(1), pp. 1–27 (1995)

STRUCTURE–PROPERTY RELATIONSHIPS IN SEGMENTED POLYVIOLOGEN IONENE ROTAXANES

DON LOVEDAY and GARTH L. WILKES*

Polymer Materials and Interfaces Laboratory
Chemical Engineering Department

MUKESH C. BHEDA, YA. X. SHEN, and HARRY W. GIBSON

Chemistry Department

Virginia Polytechnic Institute and State University
Blacksburg, Virginia 24061

ABSTRACT

The first structure–property relationships are reported for segmented polyrotaxane ionenes which possess the rotaxane moiety at the hard segment. These ionenes are based on PTMO/MDI (PTMO M_n of 650, 1000, or 2000 daltons) as the elastomeric segment and paraquat hard segments with either PF_6^- or Br^- as the counterion. GPC indicates that these ionenes have a highly variable architecture with respect to the placement of the ionene hard segment. SAXS also supports the notion of a randomly placed hard segment because the interionic domain *d* spacings are not predictable or consistent. SAXS also shows there are few "lone multiplets" in the PF_6^- derivative whereas there are considerable numbers of isolated ion pairs in the Br^- ion-exchanged ionenes. Tensile testing shows that the PTMO-1000 and PTMO-2000 materials are elastomeric with good properties, but the PTMO-650 ionene is not elastomeric with the ionic hard segment as a continuous phase. Dynamic mechanical tests also indicate that these segmented ionenes are phase separated with two transitions. TGA indicates that the rotaxane derivative is stable to higher temperatures than the nonrotaxane analog.

Although the observed structure-property relationships suggest that these systems are generally varied in the placement of the paraquat hard segments, it is clear that the rotaxane moiety increases the elastic modulus and increases thermal stability.

INTRODUCTION

Novel molecular composites called polyrotaxanes have appeared recently wherein a linear macromolecule "threads" a macrocycle [1–10], as shown in Fig. 1. In general, this "threading" is an equilibrium process but can be controlled by specific interactions such as host–guest complexation as in the case of polyrotaxane ionenes to be discussed. These polymers represent a novel molecular architecture as compared to conventional polymers where there is no intramolecular interaction of such a topologically specialized nature. Further, polyviologen ionenes represent a unique subclass of segmented ionomers since the viologen may participate in redox chemistry [11].

Here, these unique structures are brought together in the form of polyviologen rotaxane ionenes [3]. In this report we consider a specific type of polyrotaxane ionene based on a polyurethane ionene architecture and a model analog (without the macrocycle), shown in Fig. 2. In the polyrotaxane ionenes ("rotaxane") shown in the figure, poly(tetramethylene oxide) (PTMO) segments alternate with paraquat diol hard segments as in traditional segmented ionenes. Unlike traditional segmented ionenes, the ionene unit is also encircled by a macrocycle, bis(*p*-phenylene)-30-crown-10, at the hard segment loci. The paraquat hard segment and its associated

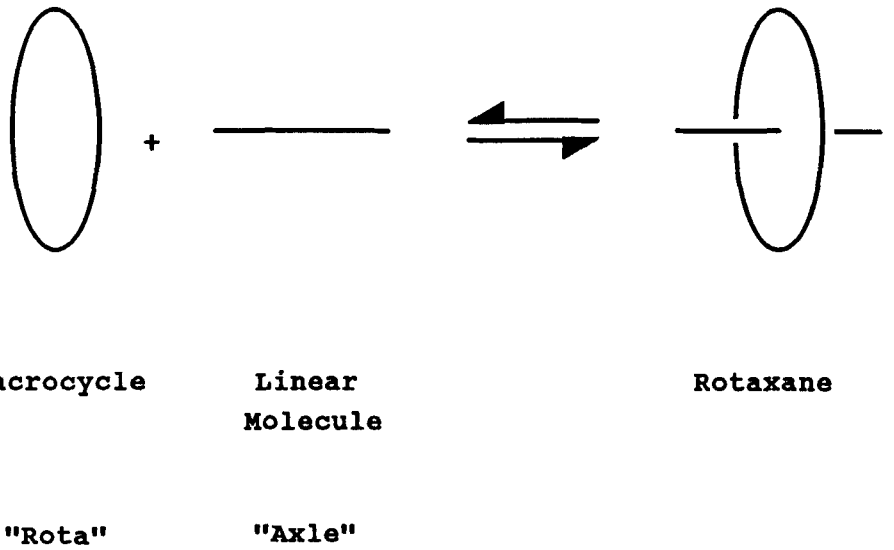

FIG. 1. The equilibrium relationship governing the threading process in polyrotaxanes. Specific interactions, such as the host–guest complex in the polyrotaxane ionenes, drive the equilibrium strongly to the right.

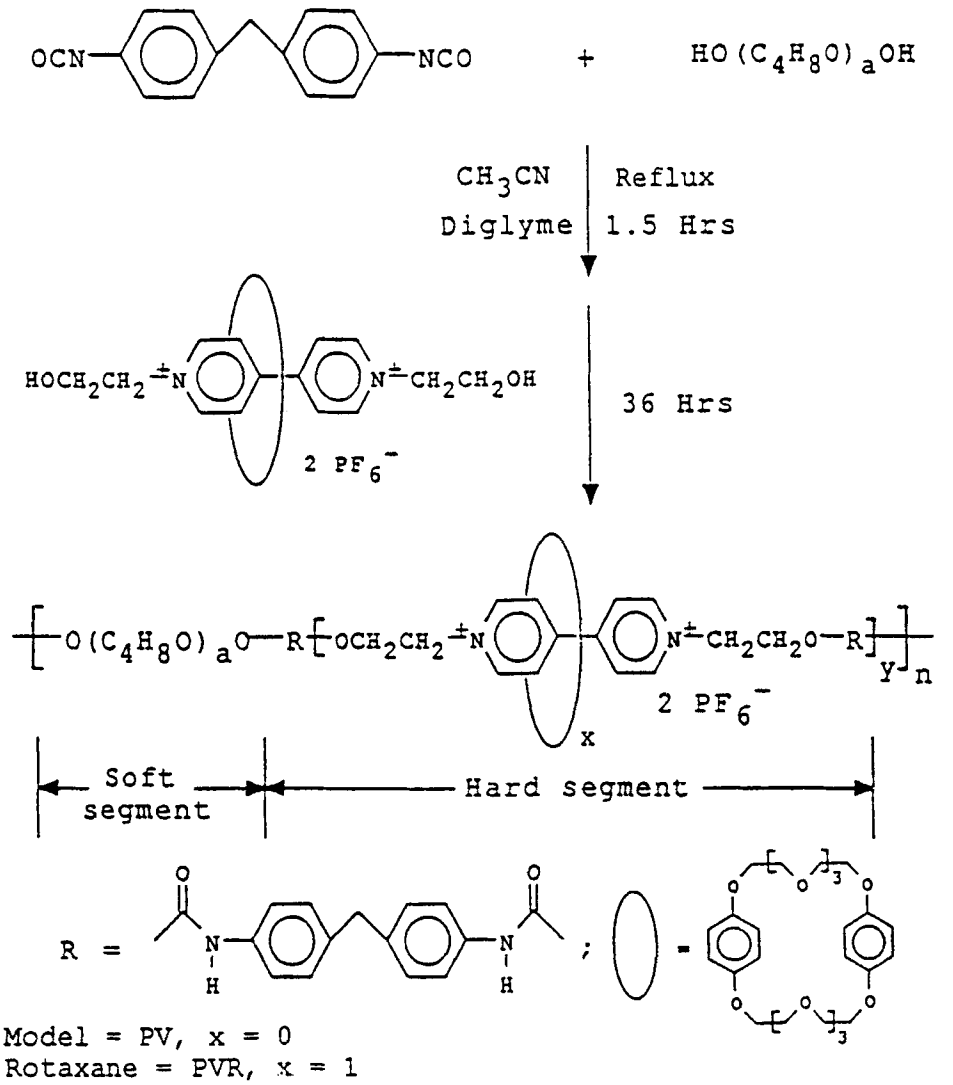

FIG. 2. The reaction scheme. x = 0 for model, x = 1 for rotaxane. Note the use of the scheme of A (PTMO) + B (MDI) to form a prepolymer, then B[A-B]$_n$ + C (paraquat diol) to form the final polymer.

macrocycle are a fixed species, their interaction being the result of a host-guest charge transfer complex between the electron depleted π-orbitals of the pyridinium units and the electron-rich phenylene moieties of the macrocycle [7]. This strongly bound interaction is in contrast to other polyrotaxanes that have been studied, where the equilibrium behavior of Fig. 1 is not shifted strongly to the right by a specific interaction. In other rotaxanes, blocking groups must be attached to the ends of the macromolecule to prevent the macrocycle from "slipping off" [1]. These polyrotaxanes are "assembled" from the rotaxane monomer and the soft segment.

For comparative purposes, we have also prepared the nonrotaxane ("model") species with no macrocycles. These "model" species possess many similarities to polyviologen ionenes previously studied in our laboratory [12, 13] and others [14].

In such a novel molecular architecture, the question arises as to the effect that the rotaxane moiety will have on the ionene's ionic interactions and how this may influence ordering in the "ionic domain." A related question is how the ordering of the "ionic domain" might then influence properties. Certainly, the inclusion of the rotaxane moiety elevates these materials to a new level of architectural complexity, above that of segmented ionenes studied previously. Segmented PTMO/1,4-bis(bromomethyl)benzene-based ionenes which we studied before exhibited the traditional aggregation of ionic groups to form a separate ionic domain morphology at low volume fractions of the ionic moiety [12]. In special cases it is known from our previous work [12] that segmented ionene polyviologens may even possess an ordered morphology of rodlike ionic domains dispersed in the matrix when the volume fraction of the ionene hard segment is only ca. 6% or greater. These materials were composed of PTMO soft segments (M_ns of 1400 or 1800) and 1,4-bis(bromomethyl)benzene hard segments with Br^- as the counterion, and they were cast from $CHCl_3$. Similar ionenes (with bipyridinium hard segments and Br^- counterions) we have examined exhibited a single peak, though not such long-range ordering [15], in small-angle x-ray scattering (SAXS) studies. The objectives in the present paper are to examine the effect of the rotaxane moiety on ordering and to compare the behavior of such systems to the nonrotaxane "model" systems. Further, we examine the effect on SAXS behavior of replacing the PF_6^- (hexafluorophosphate) counterion (recall Fig. 2) with the smaller and more electron dense Br^- anion. As well, we also discuss the important aspect of chain architecture in these segmented ionene materials and seek to relate architectural randomness to properties. Through this paper we establish the first report of the structure–property relationships of segmented polyrotaxane ionenes.

MATERIALS

The materials synthesized for this study consist of two basic types, a polyrotaxane ionene ("rotaxane") and a polyurethane ionene ("model"). A general synthetic method for the polyrotaxane ionenes, by Gibson et al., is described elsewhere [7, 16]. The PTMO M_n was varied from 650 to 1000 to 2000 daltons, providing a range of ionic content and, in the case of the rotaxane, expression of the rotaxane moiety. The compositions and designations of the various polymers are found in Table 1. The nomenclature is: (PV(R)-M_n, where PV = polyviologen, PVR = polyviologen rotaxane, and M_n is the PTMO M_n. To distinguish between the two versions of the PTMO-2000 materials examined here, two additional PTMO-2000 materials are designated PV-2k and PVR-2k. (The PV-2k and PVR-2k materials differ from the other PTMO-2000 materials in that they were polymerized longer to increase the molecular weight of the final polymer.) The polymers were dissolved in THF overnight, cast into Teflon molds, and allowed to dry overnight. The resultant films were dried in vacuo at 90°C for 24 hours to remove residual THF. For selected samples, the ion-exchange process was conducted by dissolving the PF_6^- material in THF (ca. 10 wt% polymer) and then precipitating the solution into a vigorously

TABLE 1. Characteristics of the Ionenes Used in this Study [PTMO = poly(tetramethylene oxide); BPP = bis-*p*-phenylene-30-crown-10, the macrocycle; MDI = methylene bis(phenylenediisocyanate); PQ = paraquat diol, the viologen unit]

Name	Soft segment, g/mol	Hard segment	BPP/PQ, (M/M)[a]	PTMO:MDI: PQ, (M:M:M)[a]	Hard segment, wt%[b]	BPP, wt%[b]
PV-650	650	MDI/PQ	0.00	1.02:2.02:1.00	61	0
PVR-650	650	MDI/(PQ/BPP)	0.99	1.01:2.01:1.00	61	24
PV-1000	1000	MDI/PQ	0.00	1.22:2.22:1.00	47	0
PVR-1000	1000	MDI/(PQ/BPP)	0.98	1.46:2.46:1.00	45	17
PV-2000	2000	MDI/PQ	0.00	1.00:2.00:1.00	34	0
PVR-2000	2000	MDI/(PQ/BPP)	1.00	1.00:2.00:1.00	34	15

[a]Determined by NMR.
[b]Based on molar proportions from NMR.
M = mole.

stirred water/NaBr solution. The precipitate was collected and dried, and a film was formed from this, as above, using THF and drying as before. All of the films were hydrophilic, absorbing between 10 (for the PTMO-2000 materials) and 30 (for the PTMO-650 materials) wt% water in 6-hour immersion experiments. Thus, due to the hydrophilic nature of the materials, the driest possible conditions were used at all times, such as storage of the films in a desiccator and rapidly performing tests at ambient conditions, e.g., tensile testing. When possible, a dry atmosphere was used, such as an N_2 purge, e.g., in DMS (dynamic mechanical spectroscopy).

EXPERIMENTAL

Small-angle x-ray scattering profiles of the films were taken on a slit collimated compact Kratky camera equipped with an M. Braun position sensitive detector. The x-ray source was a Philips PW-1729 generator providing Ni-filtered CuK_α radiation ($\lambda = 0.154$ nm). WAXS were taken in a Statton camera in vacuo, mounted on a Philips PW-1720 x-ray generator. The Ni-filtered incident beam of CuK_α radiation was doubly collimated to 0.015 in. diameter. The dynamic mechanical analyses were performed with a Seiko DMS-210 at a heating rate of 2°C/min under nitrogen purge. Thermogravimetry was performed using a Seiko TG/DTA-100 at 10°C/min under nitrogen purge. The mechanical properties were determined on micro-"dogbones" with an Instron model 1121 at ambient conditions (25°C) and an elongation rate of 100%/min, unless otherwise noted. Gel permeation chromatograms of the PTMO/MDI prepolymer were determined in THF on a Waters column, and MWDs were determined using PS standards. FT-IR spectra were recorded using a Nicolet FT-IR-510.

RESULTS

Characterization

In this work the issue of chain architecture (MWD of the elastomeric segment and chain topology) is of great importance. It is important to note here that these materials do not have single PTMO oligomers as the soft segments, but have PTMO/MDI *elastomeric segments* between the ionene hard segments (Fig. 3). In an effort to elucidate the MWD of the elastomeric segments between the ionene hard segments, GPC was performed on the PTMO/MDI prepolymer quenched with MeOH.

The GPC data were collected to ascertain the polydispersity of the PTMO/MDI prepolymer (the elastomeric segments in the final polymer) in a typical PTMO-2000 material. This question stems from the fact that the PTMO diol and the MDI chain extender were added to form a prepolymer all at the same time (see Fig. 2). To minimize the production of PTMO/MDI polymer, the oligomer may be added dropwise to an excess of MDI in solution, greatly maximizing the likelihood of only endcapping the PTMO segments over that of chain extension (polymerization). The method that was employed in this study, on the other hand, results in a significant fraction of polymeric diisocyanate, which is then reacted with the para-

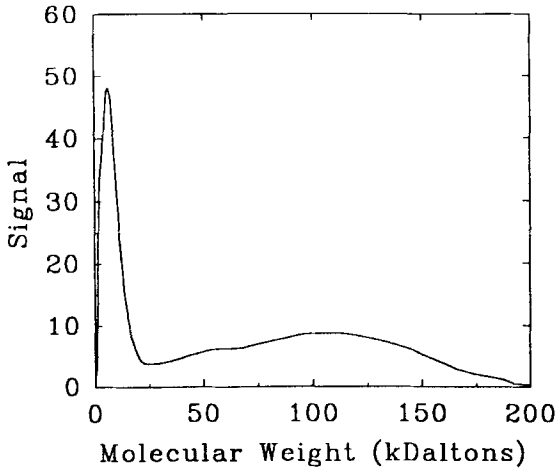

FIG. 3. Gel permeation chromatogram of the methanol-terminated prepolymer, MDI[PTMO-MDI]$_n$, showing the detector signal as a function of molecular weight.

quat diol to form the ionene. This polyurethane has both the traditional PTMO soft segments and single MDI hard segments in its "elastomeric segment" between the ionene moieties, as noted in the preceding paragraph. For GPC, a sample of this PTMO-MDI (based on PTMO-2000) prepolymer was prepared and then terminated with MeOH instead of the normal polymerization route using the viologen (paraquat diol) hard segment. The MWD of this methanol-quenched PTMO-2000/MDI prepolymer is shown in Fig. 3. It is clear that the method of synthesis results in a prepolymer which has a very broad range of sequence sizes in the PTMO-MDI elastomeric unit between the ionene hard segments. This is in contrast to the notion of a well-defined soft segment, which can be a single PTMO (or other) oligomer. Thus, the ionene units are not located at well-defined intervals along the chain but are, instead, at irregular locations along the chain. In addition, the formation of polymeric segments, such as "50-mers," of the PTMO-MDI prepolymer implies that there is some residual MDI present in the reaction mixture prior to the addition of the paraquat diol ionene monomer. As will be shown later, these aspects of the synthetic method are manifest in the structure-property relationships.

It was also noted that there was a significant gel fraction in some materials (PV-2k and PVR-2k, Table 1). These materials, in solution, yielded approximately 30 to 40 volume percent gel. FT-IR was performed on this pair of PTMO-2000 ionenes (a model and a rotaxane) which were generated according to the reaction scheme in Fig. 2 (designated PV-2k and PVR-2k, respectively) and the recipes shown in Table 1. These polymers were dissolved in THF and cast onto KBr disks, then thoroughly dried in vacuo at ca. 80°C. Portions of the FT-IR spectra of both the model and rotaxane are shown in Fig. 4. An appreciable peak is present in the region of 1715–19 cm^{-1}, which is often attributed to the biuret and allophanate trifunctional linkages in polyurethanes [17]. The neighboring urethane peak at 1733 cm^{-1} gives some indication of the relative amount of the trifunctional linkages in the system. These trifunctional linkages are thought to be the result of polymeriza-

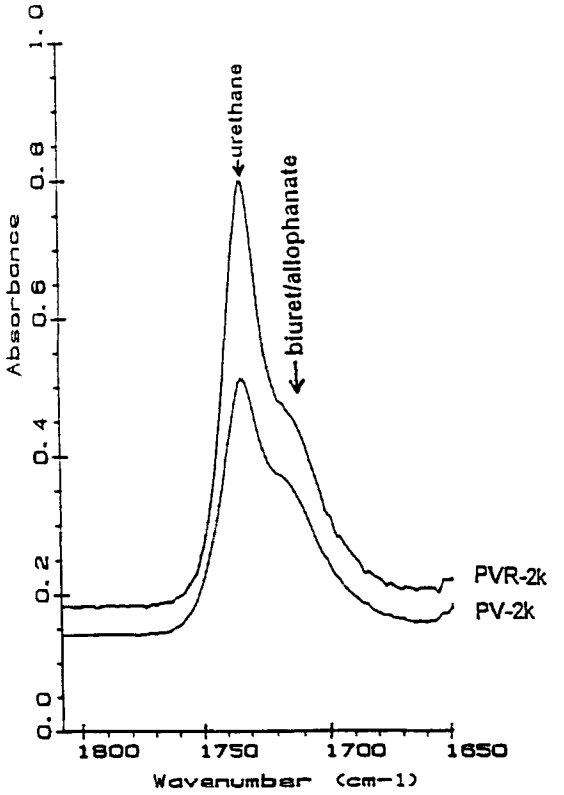

FIG. 4. FT-IR spectra of the region containing the peaks associated with the allophanate/biuret (ca. 1715 to 1719 cm^{-1}) and the urethane link (ca. 1733 cm^{-1}). Note the relative areas of the trifunctional biuret/allophanate linkage peak versus the urethane peak.

tion at temperatures which were in the region of 110 to 125°C during at least part of the polymerization regime, as higher temperatures are known to encourage the formation of the trifunctional linkages [17]. However, it is not known what gel fraction was present in the other ionenes (PV-650, PVR-650, PV-1000, PVR-1000, PV-2000, PVR-2000) in this study, as they were vacuum filtered as a part of the purification process. It is known that there was some gel in the original materials, as the record of filtrations suggest polymer was lost which should have been recoverable by filtration. The presence of these trifunctional linkages will also influence the properties of the system, as will be evident later.

Small-Angle X-Ray Scattering (SAXS)

The SAXS profiles of the THF-cast PF_6^- films are shown in Figs. 5a–c for the three PTMO molecular weights (M_ns). The slit-smeared intensity is plotted as a function of the angular variable, s, where $s = (2/\lambda)\sin(\Theta)$, Θ being one-half the radial scattering angle. In each case a peak is present in the profile; this peak is customarily taken as evidence of phase separation with the ionic aggregates distrib-

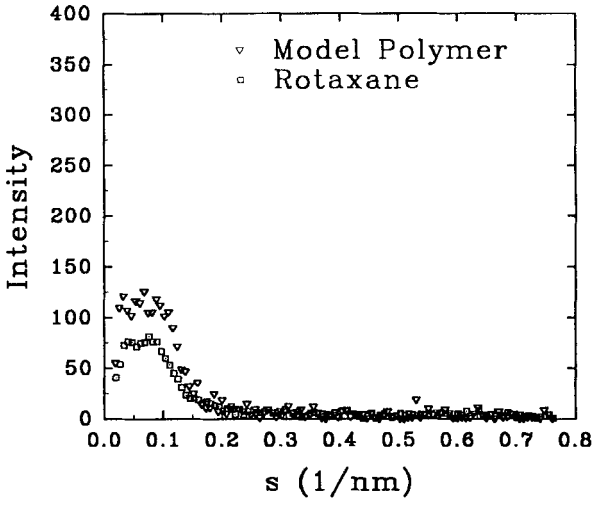

FIG. 5a. Smeared SAXS profiles of the PTMO-650 PF_6^- polyviologen ionenes. Intensity is in arbitrary units.

uted in the matrix. The corresponding smeared *d* spacings were determined from the peaks in these smeared profiles and are reported in Table 2. The lack of a systematic increase in the value of the *d* spacing is at first a bit puzzling, as one might expect that the spacing would increase with increasing PTMO M_n [12]. In an effort to elucidate the reason for the lack of systematic change in the spacing, the PF_6^- was exchanged for the Br^- anion, which provides much better x-ray contrast via its higher electron density. This exchange of ions could also provide a way to

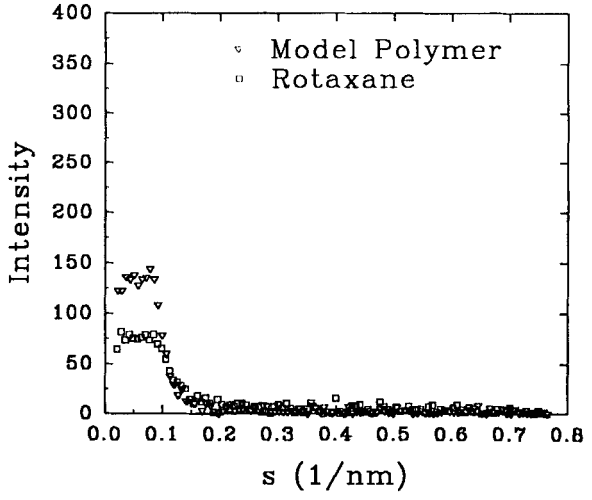

FIG. 5b. Smeared SAXS profiles of the PTMO-1000 PF_6^- polyviologen ionenes. Intensity is in arbitrary units.

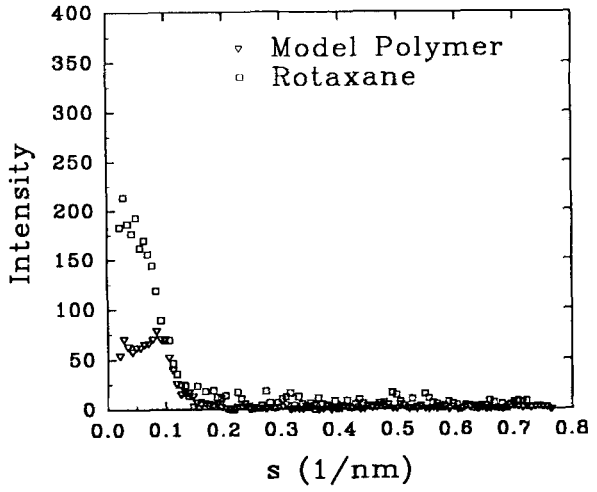

FIG. 5c. Smeared SAXS profiles of the PTMO-2000 PF_6^- polyviologen ionenes. Intensity is in arbitrary units.

compare the polyrotaxane materials and the brominated PTMO-based ionenes which were previously studied in our laboratory [12, 15]. The result is shown in Figs. 6a–c. In each portion of the figure it is seen that the small-angle x-ray region contrast is greatly enhanced by the ion exchange. This enhanced contrast is evident from the sharpened peak in the Br^- profile. Even with the exchange process, though, the *d* spacings are still unsystematic with PTMO molecular weight, as shown in Table 2. Still, the ion-exchange process affects the interdomain spacing. For example, the *d* spacing of the PV-650 materials changes from 15.2 nm for the PF_6^- to 11.5 nm for the Br^- ionene. The PVR-650 materials also show such an effect, with the PF_6^- ionene having a spacing of 14.9 nm and the Br^- ionene a spacing of 11.5 nm, the same as the PV-650 Br^- ionene. In general, the *d* spacings of the Br^- materials are slightly lower than the corresponding *d* spacings for the PF_6^- materials, except the model PTMO-2000 ionenes (where the Br^- has a slightly higher spacing, 13.7 nm, than the PF_6^- ionene, 10.8 nm). Our speculation is that the

TABLE 2. SAXS *d* Spacings Determined from Smeared Profiles of Polyviologen Ionenes

Sample name	PF_6^- *d*, nm	Br^- *d*, nm
PV-650	15.2	11.5
PVR-650	14.9	11.5
PV-1000	17.0	14.9
PVR-1000	16.6	13.2
PV-2000	10.8	13.7
PVR-2000	14.3	12.5

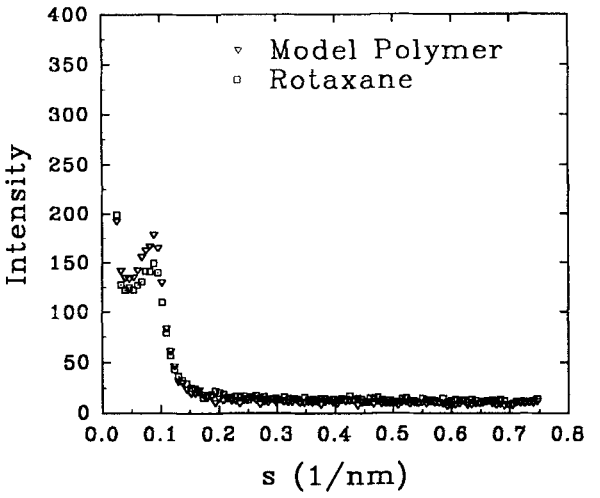

FIG. 6a. Smeared SAXS profiles of the PTMO-650 Br^- polyviologen ionenes. Intensity is in arbitrary units.

smaller Br ion may promote better phase separation, and perhaps more packing order, versus the bulky PF_6^- counterion.

In addition, the *d* spacings obtained for the Br^- materials are much higher than the primary *d* spacings obtained in the SAXS profiles of well-defined PTMO segmented ionene materials, studied previously in our laboratory [12, 13, 18]. Feng et al. found the smeared *d* spacings of PTMO-1800 and PTMO-2600 materials to be 7.0 and 7.8 nm, respectively [18]. The smeared *d* spacing of the PV-2000 Br^-

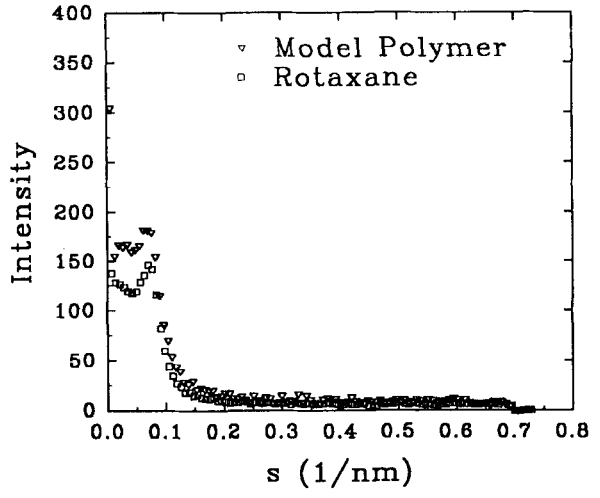

FIG. 6b. Smeared SAXS profiles of the PTMO-1000 Br^- polyviologen ionenes. Intensity is in arbitrary units.

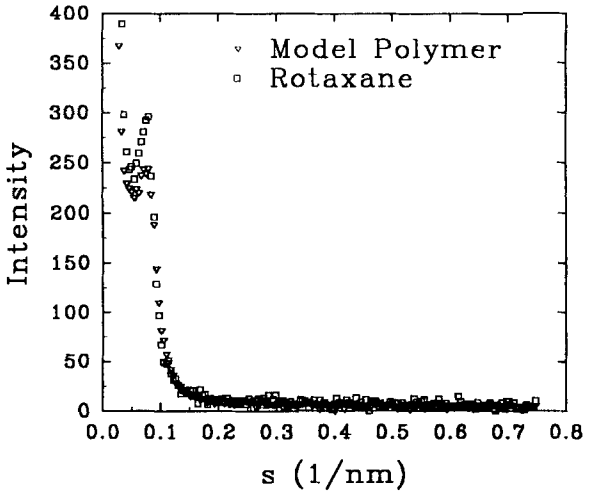

FIG. 6c. Smeared SAXS profiles of the PTMO-2000 Br^- polyviologen ionenes. Intensity is in arbitrary units.

ionene (13.7 nm, Table 2) is almost double that of Feng's PTMO-1800 material and well above that of the PTMO-2600 ionene, too. Abouzahr and Wilkes [19] studied segmented, nonionic polyurethane-ureas based on PTMO and 2,4-toluenediisocyanate (TDI), with ethylenediamine as the linkage in the hard segment. For a PTMO-2000 polyurethane-urea of 30 wt% hard segment, the interdomain spacing (desmeared) was 14.0 nm. This is similar to our value of 13.7 nm for the smeared d of PV-2000 (with 34 wt% hard segment, Table 1). The material of Abouzahr and Wilkes was made by first "endcapping" the PTMO with 2,4-TDI, extended via 1,4-butanediol, then the hard segment was linked with ethylenediamine. The endcapping step was conducted by adding the PTMO and 2,4-TDI at the same time, as in the materials (in our case, MDI) in this study. Thus, this nonionic polyurethane-urea material should have a variable "elastomeric soft segment" length where the elastomeric soft segment is a few PTMO/2,4-TDI repeat units. In both systems the resultant architecture is relatively random, with a distribution of elastomeric segment sizes, though the average size is certainly greater than a single PTMO oligomer. As a result, greater interdomain spacings are found in these elastomeric segment materials than those obtained in the well-defined, i.e., nonrandom soft segment length, architecture studied by Venkateshwaran, Feng, and Wilkes [12, 13, 18]. The tentative soft segment length explanation for this lack of systematic change in the d spacing is elaborated further in later sections of this paper.

The Br^- profiles also exhibit the characteristic upturn in SAXS intensity as $s \rightarrow 0$ that has been attributed to the presence of "lone multiplets," as postulated by Ding and Cooper [20]. However, the PF_6^- ionenes show no such upturn as $s \rightarrow 0$, implying a lack of lone multiplets. In earlier studies of PTMO-dihalide ionenes of similar architecture in our laboratory [12], no such upturn was encountered in the SAXS profiles, leading to the conclusion that there were no ionic segment domains which were of the lone multiplet type. This lack of lone multiplets was attributed to

stoichiometry in these materials synthesized from α,ω-bis(dimethylamino) PTMO and 1,4-bis(bromomethyl)benzene, as the bromide counterion was a product of the reaction joining the hard and soft segments, resulting in a 1:1 ratio of N^+ ions to Br^- counterions. (Generally in other ionenes and ionomers, the counterion is put into the system by a post-synthesis neutralization and an excess of the neutralization compound may be left in the system or the product salt may not be completely removed.) This, along with the very well-defined location of the ionene unit on the chain, gave a great degree of order in the ionene hard segment domain [12]. In the polyrotaxane Br^- ionenes, it appears that there is a sizable population of species which exhibit lone multiplet-type scattering. This is in contrast to both the materials we have studied previously [12] and the current PF_6^- materials, wherein there is no upturn as $s \rightarrow 0$. This would seem to lead to a contradictory situation, but if the efficiency of the exchange is not 1:1, then there could potentially be residual $NaPF_6$ or NaBr in the matrix, contributing to the very long range correlation scattering as $s \rightarrow 0$. We speculate that the ion exchange is the cause of the upturn in $I(s)$ as $s \rightarrow 0$ in the Br^- materials, since the exchange is the only difference in the two sets of materials.

Mechanical Properties of Model and Rotaxane Ionenes

The tensile stress–strain profiles of the PF_6^- ionenes are shown in Figs. 7a–c. The tensile properties of the PF_6^- materials are summarized in Table 3. In the case of the rotaxane of PTMO M_n 650, there is reproducible yielding behavior. This yielding behavior is certainly the result of the presence of the macrocycle, since the behavior is not observed in the model polymer of the same PTMO M_n. Additionally, the proportion of ionic segments in the PTMO-650 materials is high (84 wt% in rotaxane, 64 wt% in model; see Table 1), and thus the ionic domain component largely

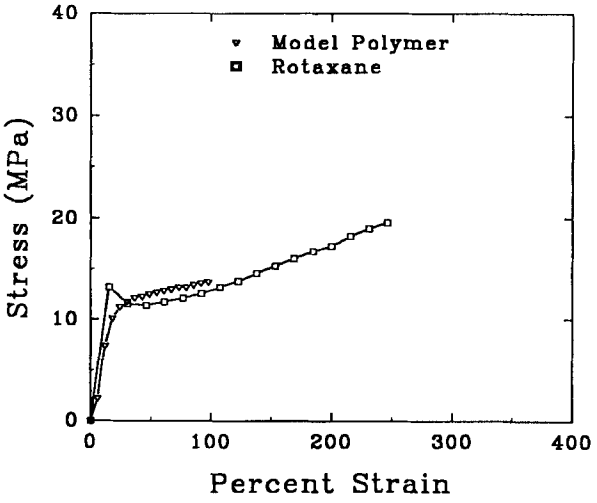

FIG. 7a. Representative tensile test profiles of the PTMO-650 PF_6^- ionenes. Rate = 100%/min.

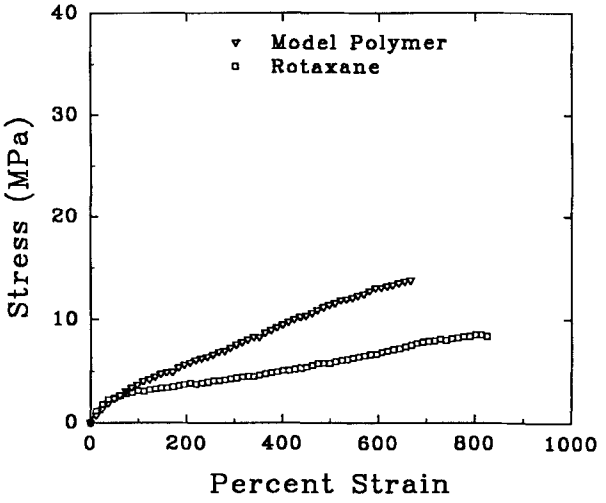

FIG. 7b. Representative tensile test profiles of the PTMO-1000 PF_6^- ionenes. Rate = 100%/min.

determines the properties, and is likely the continuous phase in the material. Thus, the high moduli of the PV-650 and PVR-650 materials (8.1 and 23 MPa, respectively) are to be anticipated when the hard component is continuous. The general trend of higher elongation-to-break and lower modulus with increasing PTMO M_n (i.e., decreasing ionic content) is present. This is expected, as the expres-

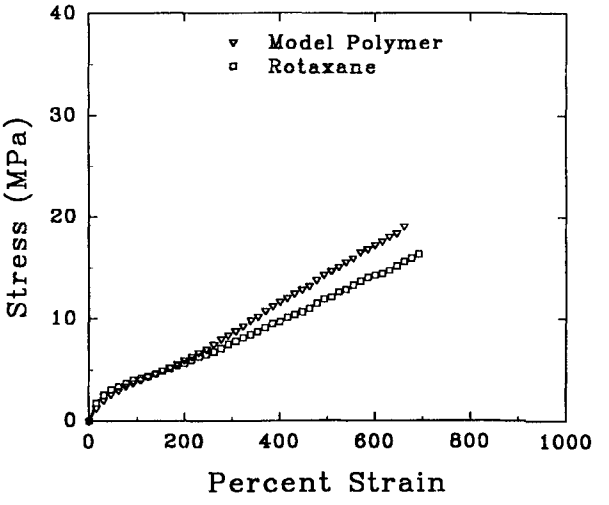

FIG. 7c. Representative tensile test profiles of the PTMO-2000 PF_6^- ionenes. Rate = 100%/min.

TABLE 3. Tensile Properties of PF_6^- Polyviologen Ionenes. Tested at Ambient Conditions and 100%/min.

Name	E, MPa	Elongation at break, %	Stress at break, MPa
PV-650	8.1	169	23
PVR-650	23	114	20
PV-1000	0.6	588	21
PVR-1000	1.6	625	17
PV-2000	0.7	508	20
PVR-2000	1.9	432	17
PV-2k[a]	2.0	710	32
PVR-2k[a]	1.8	807	34

[a]Tested at 500%/min.

sion of the ionic moiety (hence, the amount of ionic aggregates) is also decreasing. It should also be noted that the recovery of the PTMO-650 materials was negligible while it was good in the PTMO-1000 and -2000 materials, implying that the elastomeric segment is the continuous phase in the latter two materials and the ionene hard segment is the continuous phase in the PTMO-650 materials.

From Table 3 and Figs. 7b and 7c, it is seen that the model polymers PV-1000 and PV-2000 behave in much the same way as other ionic segmented polymers [12, 13, 15], having a broad rubbery plateau, low modulus, and high elongation to break. However, when compared to the other ionene polymers previously studied in our laboratory [12, 15], the model systems exhibit poorer elongation to break and

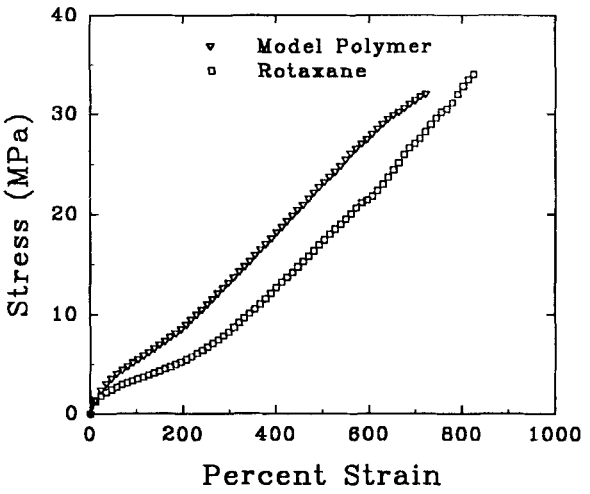

FIG. 8. Representative tensile test profiles of the PV-2K and PVR-2K materials.

breaking stress. For example, Venkateshwaran et al. found (under similar test conditions) that ionenes of architecture similar (bipyridinium hard segments, PTMO M_n of 1800) to the present model system of PTMO M_n 2000 exhibit elongation to break of ca. 1000% and stress at break of up to 40 MPa [13]. Also, Feng et al. found similar behavior in the PTMO-segmented ionenes they studied [15]. The reason for this discrepancy between the polyrotaxane ionenes and the other, well-defined segmented ionenes is not clear, though possibly due to the fact that the ionic groups are at irregular loci on the chain in the polyrotaxane ionenes, since these ionenes have PTMO/MDI elastomeric segments between the ionene units and not pure PTMO segments. Hence, the formation of the secondary level of structural ordering at a local level that may be crucial to the enhancement of properties of the system is impaired by the irregularity of ionene moiety placement. In fact, the network structure of these materials may be thought of as a very polydisperse system with the ionic aggregates forming the crosslink points. This notion is also consistent with the SAXS (and GPC) data indicating that the elastomeric segment length is not well defined. The *d* spacing varies unsystematically with PTMO M_n and is much higher than the *d* spacing found for well-defined, segmented PTMO-based ionene systems studied earlier in our laboratories [12, 13, 18]. This gives further evidence that the current materials are not, in fact, architecturally well defined.

Surprisingly, there is no distinct stress upturn at higher elongations in either the model or rotaxane. Such an upturn is common in PTMO-segmented ionenes where the soft segment is of strain crystallizable length [12, 13, 15, 18]. The stress upturn is often associated with soft-segment strain-induced crystallization, which is at least expected in the model system of PTMO M_n 2000.

To address the lack of strain hardening and poorer tensile properties than in the previous systems, newer versions of the PTMO-2000 model and rotaxane were made. The new ionenes utilized the original formulation but were polymerized for longer time periods (PV-2k and PVR-2k in Table 1). These materials do have a noticeable stress upturn and better ultimate properties. Representative tensile stress–strain profiles of the new systems are shown in Fig. 8. Note that these materials were tested at an elongation rate of 500%/min to minimize a slippage problem between the specimen and the jaws of the Instron encountered at 100%/min. (It should be noted that this slippage problem was not encountered with any other ionenes in this study.) The properties of these newer materials are much improved, but there is still only a mild degree of strain hardening.

To investigate the improved performance of the PV-2k and PVR-2k materials, wide-angle x-ray scattering (WAXS) was used to find possible differences in the strain-induced crystallization of the PTMO-2000 materials. The WAXS profiles of each of the PTMO-2000 films were taken at $\gamma = 1.0$ (unstretched) and at $\lambda = 5.5$ for 6-hour exposures. For all the unstretched PTMO-2000 model and rotaxane films, no Debye–Scherrer rings characteristic of the unoriented PTMO crystallites were observed, only the amorphous halo. The materials were then stretched to $\lambda = 5.5$, and the WAXS images are shown in Fig. 9. In the case of the model polymers PV-2000 and PV-2k, there is strain-induced crystallization only in the PV-2k material. The presence of oriented PTMO crystallites is clearly evidenced by the equatorial "spots" in Fig. 9c. The difference between these two polymers, to note again, is that the PV-2k material was allowed to polymerize for longer time than the PV-2000

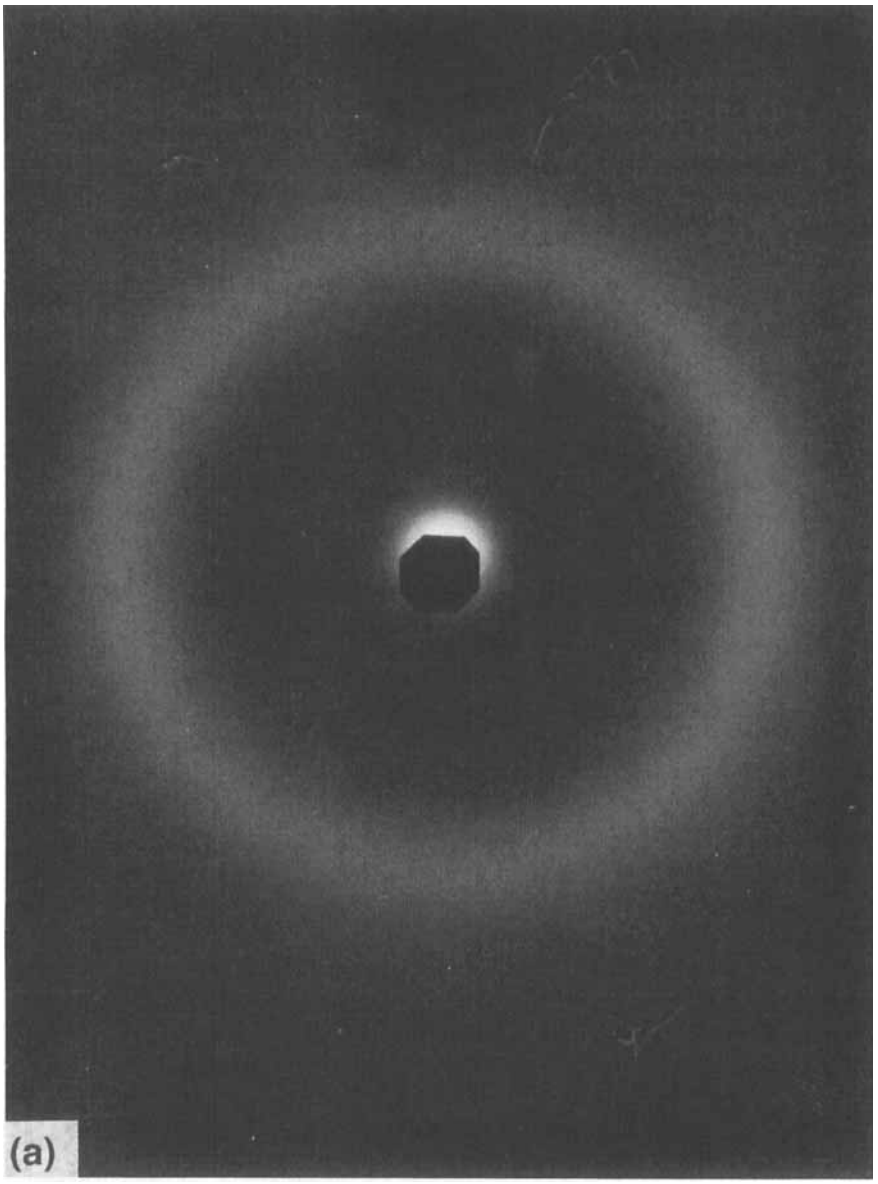

FIG. 9. WAXS patterns of the ionenes used in this study. PV-2000 (a); PVR-2000 (b); PV-2k (c); PVR-2k (d). The stretch direction is vertical.

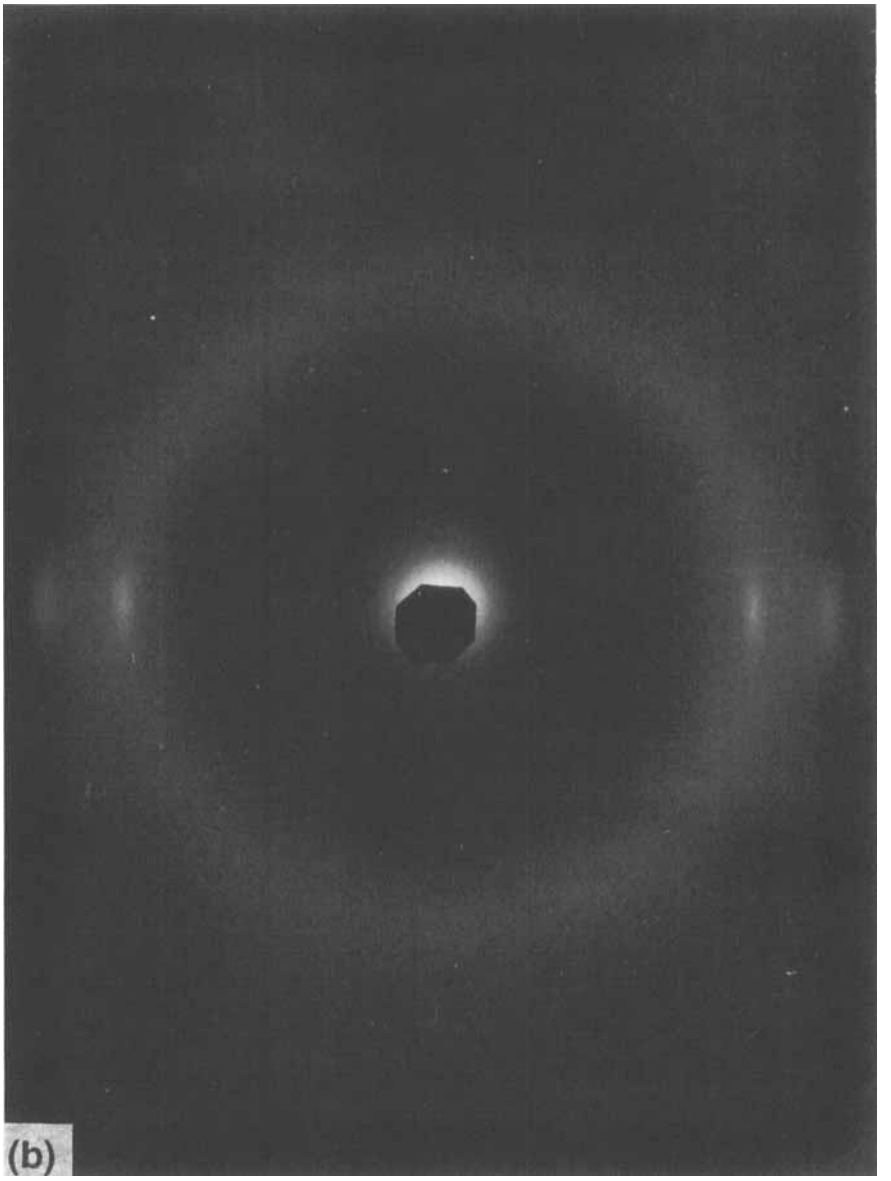

FIG. 9 (continued).

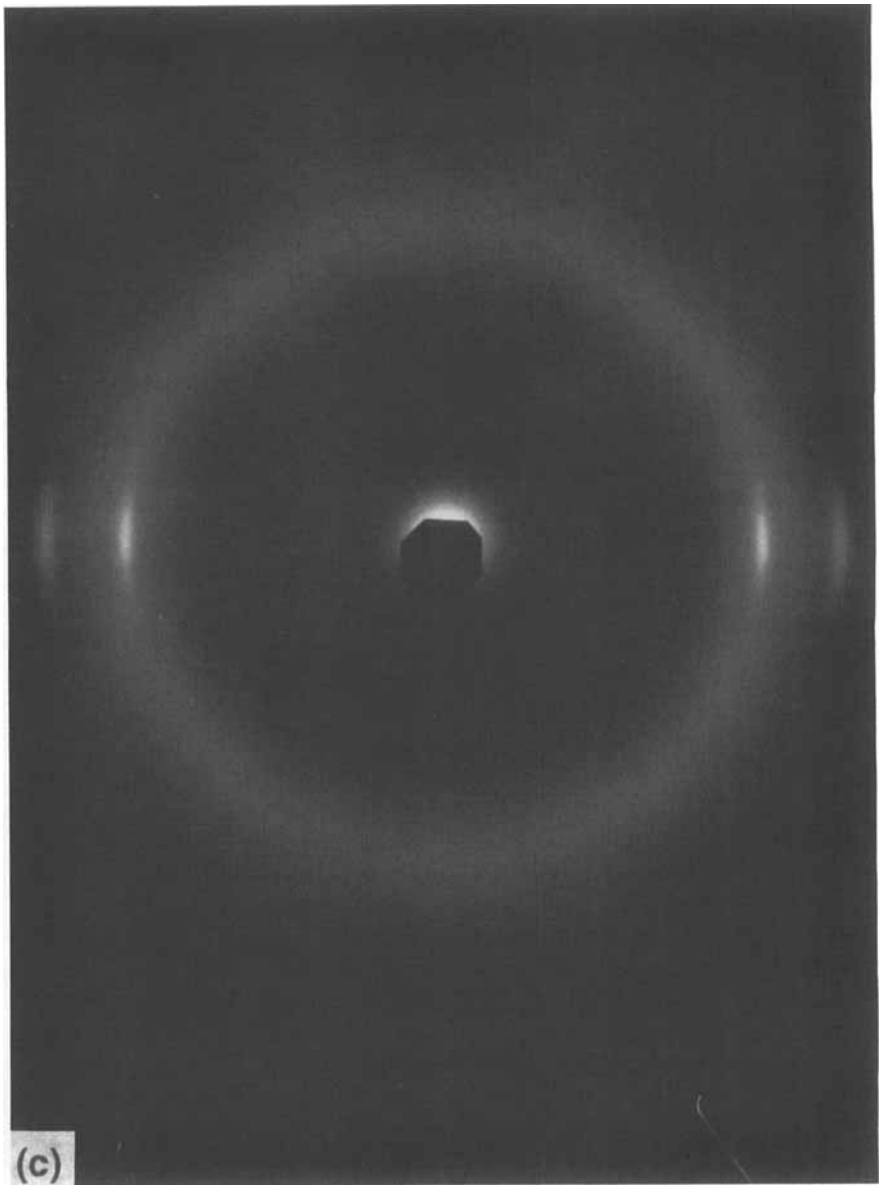

FIG. 9 (continued).

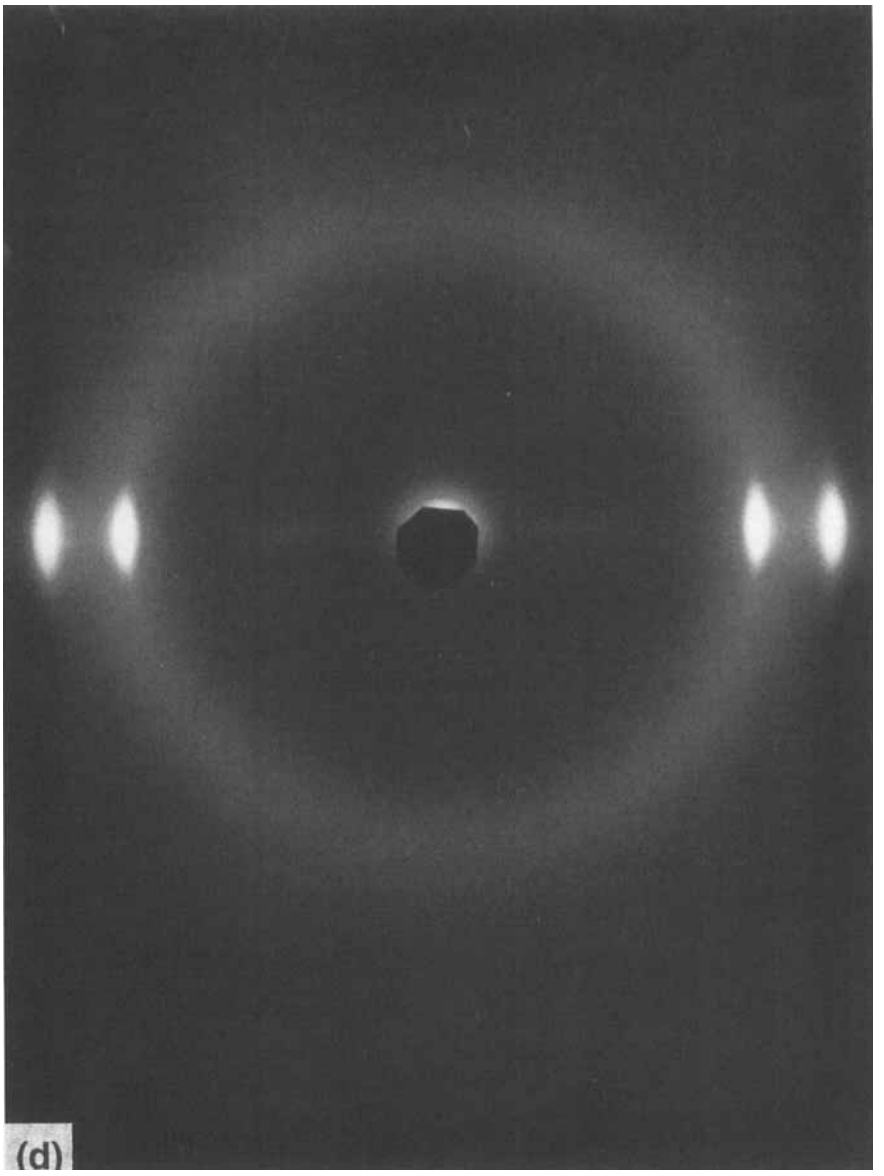

FIG. 9 (continued).

material. The crystallites present act to enhance the properties of the PV-2k, while the PV-2000 model polymer forms no crystallites and, thus, its overall properties and performance are not nearly as good as PV-2k (see Table 3, compare Figs. 7c and 8). On the other hand, the rotaxane polymers PVR-2000 and PVR-2k both show strain-induced crystallinity (Figs. 9b and 9d) at $\lambda = 5.5$. The PVR-2k material shows very strong equatorial reflections, though this difference is attributed to the thicker PVR-2k film used and not necessarily to any major difference in the amount of strain induced crystallinity.

It is possible that the slight stress upturn in the PV-2k and PVR-2k materials is not solely due to strain-induced crystallization, as well. Note that moderately crosslinked rubbers with strain crystallizable chain structures exhibit behavior similar to that found in the PV-2k and PVR-2k materials. The biuret and allophanate trifunctional linkages, evident from the FT-IR spectra of these new materials (Fig. 4), may help explain part of the slight upturn in stress and improved properties without invoking only one mechanism (e.g., crystallization) associated with strain-hardening. As well, the presence of trifunctional linkages may, in part, explain why the PV-2000 material has better properties than the PVR-2000 material (Table 3, Fig. 7c).

Dynamic-Mechanical Spectra

The 10 Hz dynamic mechanical spectra (DMS) of the PF_6^- materials are shown in Figs. 10a–c. Increasing PTMO M_n in the rotaxane ionenes causes the onset of the glass transition region (in tan δ) to move to lower temperatures, as expected. On the other hand, the model polymers' T_g at PTMO-1000 is lower than the case of PTMO-2000 and both T_g's are lower than the PTMO-650 model. This discrepancy is thought to be due to the large variation in elastomeric segment size in the PTMO-1000 and PTMO-2000 materials. The higher T_g of the PTMO-650 model (ca. -40°C) than either the PTMO-2000 (ca. -60°C) or PTMO-1000 ca. -75°C) model polymers may be due to increased constraint of the soft segment phase, as the mechanical properties and the high storage modulus suggest.

The change in the modulus of the PTMO-650 rotaxane from the glassy to the rubbery regime is smaller than that of the corresponding model. The higher modulus of the rotaxane in the rubbery regime is also indicated by the much higher tensile modulus values at room temperature (Table 3). The rotaxane and the model both exhibit high rubbery moduli (higher than the PTMO-1000 and PTMO-2000 materials, in general). These two pieces of evidence lend support to the notion that the ionic component is the more continuous phase in the PTMO-650 materials.

The rubbery plateau of the model polymer is broader than that of the rotaxane only in the case of the PTMO-1000 material. In the other cases the model polymers' rubbery response occurs over a more limited temperature range than the rotaxane. This observation can be attributed to the lack of certainty about the length of PTMO/MDI elastomeric segments in these systems. The lack of regular variation from one molecular weight of PTMO to the next can render less meaningful the magnitude and persistence of the rubbery response of any network system. This is especially true if the PTMO/MDI elastomeric segments have a very broad MWD, as Fig. 3 indicates. It should be noted that the rotaxane generally exhibits a higher

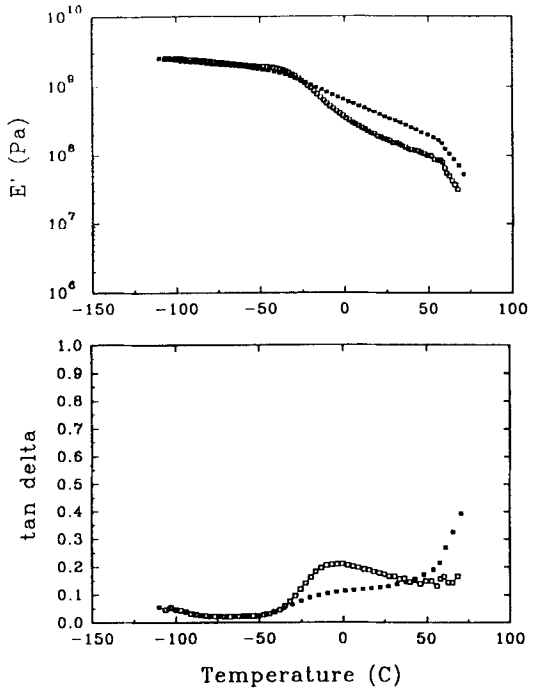

FIG. 10a. Dynamic mechanical spectra (10 Hz) for the PTMO-650 materials. Model polymer, □; rotaxane polymer, ■.

rubbery modulus (at room temperature in all cases), in accord with the tensile stress–strain results.

In the PTMO-2000 rotaxane, the crystallization and melting of the PTMO soft segment is evident by an additional plateau, from ca. −50°C to ca. 0°C. This plateau is thought to be due to PTMO crystallization. It is not clear why no such plateau is evident in the model polymer of PTMO M_n 2000. There is a small drop in the modulus of the 2000 model at ca. 0°C, but this drop is very small relative to the drop in modulus near 0°C for the rotaxane, making assignment to a crystallization-melting behavior somewhat specious.

Thermogravimetry

Thermogravimetric analyses were performed on the PF_6^- ionenes to determine the influence of the ionic moiety on the thermal stability and degradation behavior of the polymers. The results of these tests are shown in Figs. 11a–c. In Fig. 11a it can be seen that the PTMO-650 model polymers' stability is much lower than that of the corresponding rotaxane. The PTMO-650 model's onset of degradation is at a lower temperature (ca. 150°C) than the rotaxane (ca. 230°C). The model's transition at 150°C would have to be caused by a less stable species than the hard segment, though it is not known what this species might be. In addition, the PTMO-650 model has a second transition in its degradation behavior at ca. 230°C where the

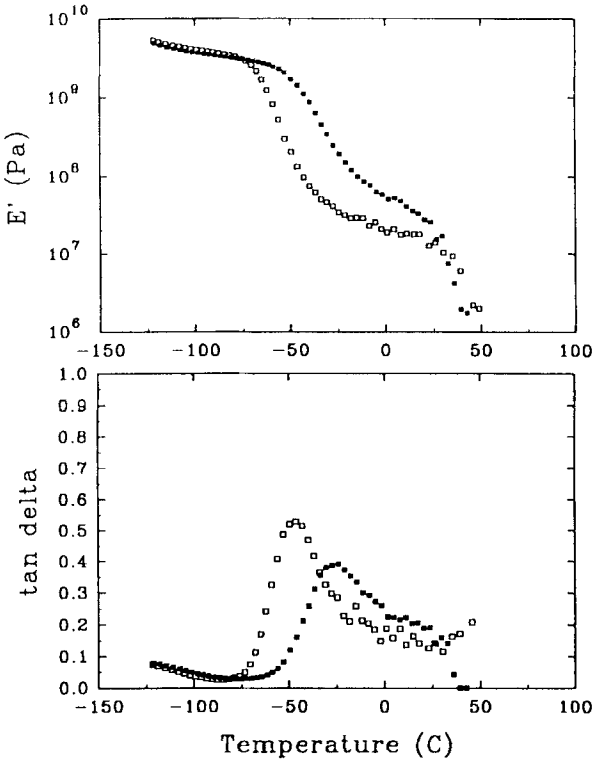

FIG. 10b. Dynamic mechanical spectra (10 Hz) for the PTMO-1000 materials. Model polymer, □; rotaxane polymer, ■.

rotaxane begins its weight loss. This suggests that the model degrades by two mechanisms.

The transition at ca. 230°C is the onset of hard segment degradation. This is apparent when one notices that the degradation between the onset and the final transition (at ca. 350°C) in each of the ionenes is roughly proportional to the original amount of hard segment in the polymer (Table 1). The amount of weight loss between the onset and the final transition is not exactly proportional in the polymers, but these are not the ideal ionenes found in Fig. 2. However, it is clear that the amount of hard segment in each case is not much different than the amount of weight loss in the intertransition region.

The presence of the rotaxane, in the case of the PTMO-650 and -2000 materials, *appears* to impart greater thermal stability versus the model polymer. The amount of degradation in the intertransition region in these two cases is less in the rotaxane than the model. This is viewed as a result of the fact that the rotaxane has the macrocycle included in its mass and, thus, seems more stable.

The final transition in these polymers occurs at ca. 360°C in the PTMO-650 materials and ca. 330°C in the PTMO-1000 and -2000 materials. This transition appears to be associated with the decomposition of the PTMO since the weight loss is, again, roughly proportional to the amount of PTMO/MDI elastomeric segment

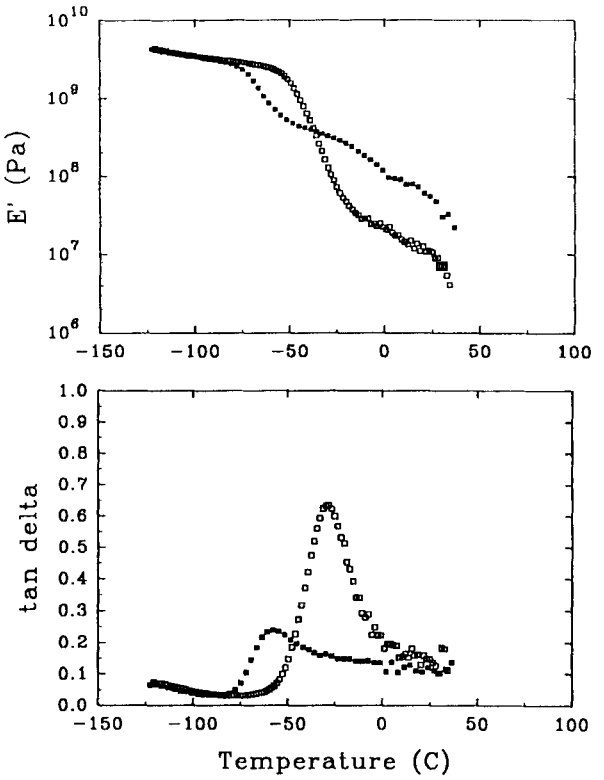

FIG. 10c. Dynamic mechanical spectra (10 Hz) for the PTMO-2000 materials. Model polymer, □; rotaxane polymer, ■.

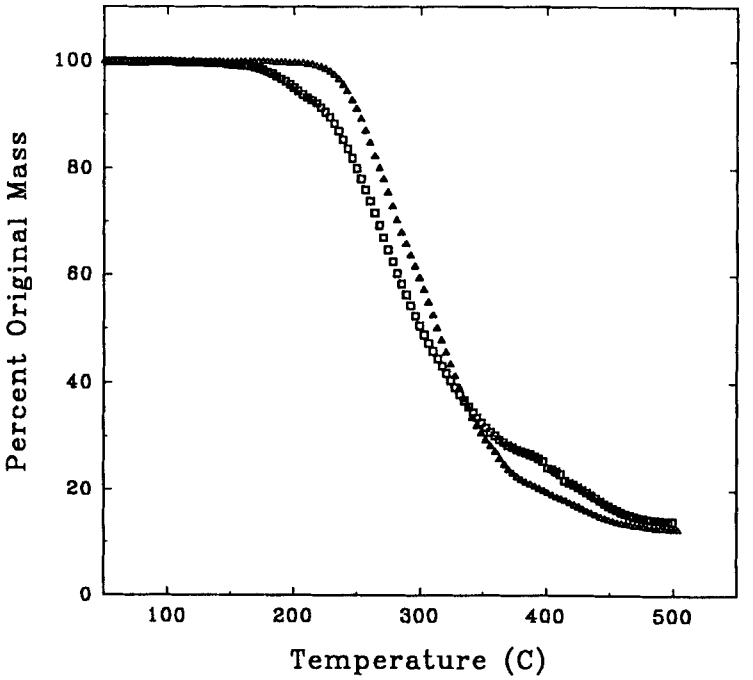

FIG. 11a. Thermogravimetric profiles of the PTMO-650 polymers showing how thermal stability is affected by the expression of the rotaxane moiety. Rotaxane, △; Model, □.

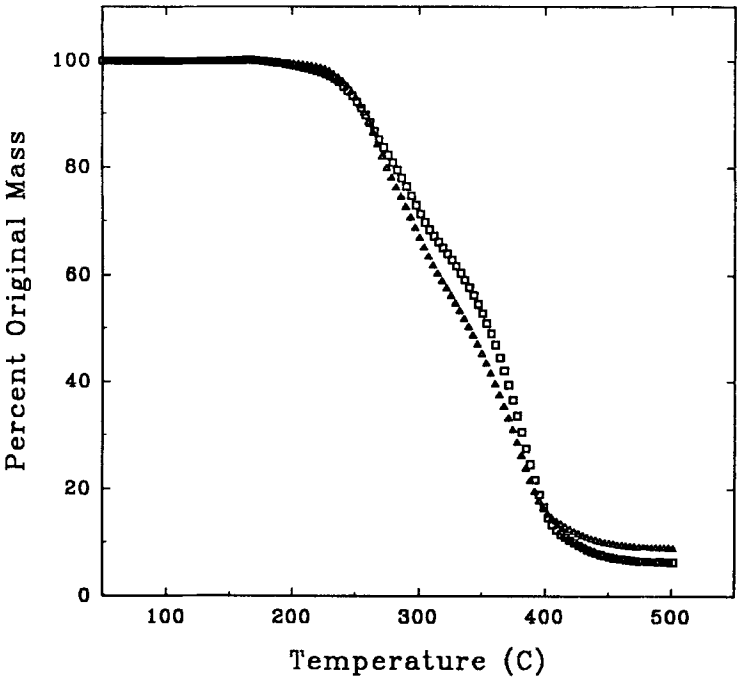

FIG. 11b. Thermogravimetric profiles of the PTMO-1000 polymers showing how thermal stability is affected by the expression of the rotaxane moiety. Rotaxane, △; Model, □.

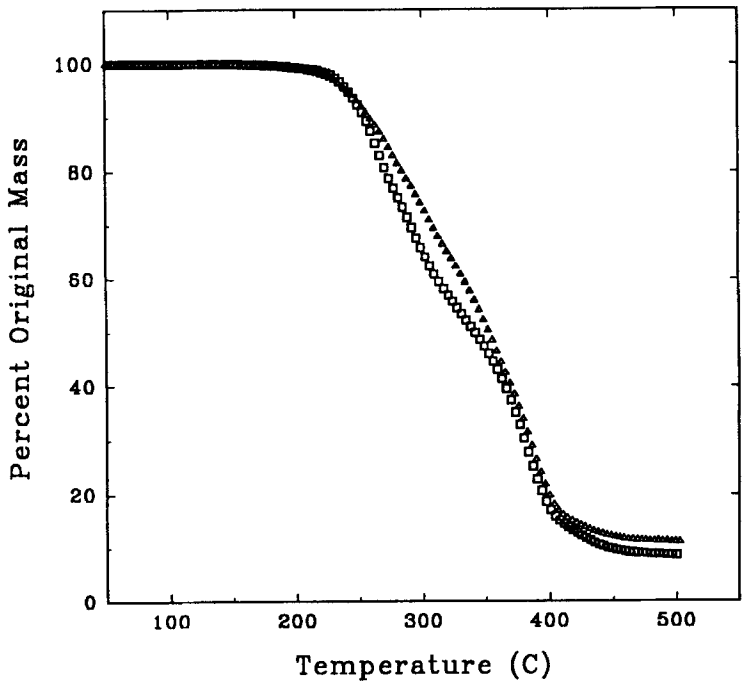

FIG. 11c. Thermogravimetric profiles of the PTMO-2000 polymers showing how thermal stability is affected by the expression of the rotaxane moiety. Rotaxane, △; Model, □.

found between the ionene hard segments in each of these materials. This final transition is at higher temperature in the PTMO-650 materials, suggesting that the remaining material is stable to a higher temperature. It is possible that the observed decomposition in the final portion of the PTMO-650 materials is simply a kinetic effect, as the amount of hard segment also is a factor in the rate of mass loss in the intertransition region and thus can determine the rate at which the decomposition proceeds.

CONCLUSIONS

This first study of segmented rotaxane ionenes has shown that they are an interesting variation on the theme of segmented, elastomeric ionenes, although they do not behave as have ionenes of well-defined molecular architecture. The GPC evidence indicates that, due to the synthetic method, these systems have a highly variable chain architecture in terms of the MWD of the PTMO/MDI elastomeric segments, as evidenced by DMS and FTIR. The presence of a peak in the SAXS profiles indicates phase separation, as is often seen in ionene systems. The exchange of Br^- for the original PF_6^- ion improved the contrast between the ionic domain and the matrix considerably, as indicated by the increased peak sharpness in the SAXS profiles. SAXS profiles indicate no systematic change in d spacing with changes in PTMO molecular weight. SAXS analysis also indicates that there are few, if any, lone multiplets in the original PF_6^- systems, but that the exchange of ions from PF_6^- to Br^- may not be 1:1 and residual salts (NaBr or $NaPF_6$) may be the cause of the increase in $I(s)$ as s approaches 0 in the ion-exchanged Br^- systems. Or, this upturn could be due to an increase in lone multiplets composed of ionic hard segments. Stress–strain measurements show that the original PTMO-1000 and -2000 materials are acceptable elastomers, though the high modulus and poor recovery of the PTMO-650 materials indicates that they are not good elastomers. WAXS indicates that while some of the PTMO-2000 materials undergo strain-induced crystallization, which enhances ultimate properties, some materials may owe part of their performance to the presence of covalent, trifunctional crosslinks, as shown by FTIR. DMS indicates that the ionene hard segment is the continuous phase in the PTMO-650 materials and is the dispersed phase in the PTMO-1000 and PTMO-2000 systems. DMS also shows that the rubbery plateau modulus of the rotaxane is higher than that of the model for each PTMO M_n. TGA supports the notion that the chain architecture is varied, since systematic changes were not observed for thermal transitions with respect to PTMO M_n. However, TGA results generally correlate with the relative amount of each species known to be present. The thermal stability of these materials appears to be enhanced by the macrocycle, though at a point where the material has already degraded beyond use. Further studies on these specific materials are not anticipated, though work with the unique macromolecule/macrocycle motif is expected to continue, especially if the ideal systems of Fig. 2 might be achieved.

ACKNOWLEDGMENTS

M.C.B., Y.X.S., and H.W.G. acknowledge support of their contributions to this work by the National Science Foundation, Division of Materials Research, Polymers Program through Grants DMR-87-12428 and DMR-90-15724.

REFERENCES

[1] (a) H. W. Gibson, M. Bheda, P. Engen, Y. X. Shen, J. Sze, C. Wu, S. Joardar, T. C. Ward, and P. R. Lecavalier, *Makromol. Chem., Macromol. Symp., 42/43*, 395 (1991); (b) H. W. Gibson and H. Marand, *Adv. Mater., 5*, 11 (1993); H. W. Gibson, P. Engen, and M. Bheda, *Prog. Polym. Sci.*, In Press.

[2] C. Wu, M. Bheda, C. Lim, Y. X. Shen, J. Sze, and H. W. Gibson, *Polym. Commun., 32*, 204 (1991).

[3] H. W. Gibson, C. Wu, Y. X. Shen, M. Bheda, J. Sze, P. Engen, A. Prasad, H. Marand, D. Loveday, and G. L. Wilkes, *Polym. Prepr. (Am. Chem. Soc., Div. Polym. Chem.), 32*(3), 637 (1991). This is a preliminary description of the present results.

[4] M. Born and H. Ritter, *Makromol. Chem., Rapid Commun., 12*, 471 (1991).

[5] G. Wenz and B. Keller, *Angew. Chem., Int. Ed. Engl., 31*, 197 (1992).

[6] J. Sze and H. W. Gibson, *Polym. Prepr. (Am. Chem. Soc., Div. Polym. Chem.), 33*(2), 331 (1992).

[7] Y. X. Shen, P. T. Engen, M. A. G. Berg, J. S. Merola and H. W. Gibson, *Macromolecules, 25*, 2786 (1992).

[8] A. Harada, J. Li, and M. Kamachi, *Nature, 356*, 325 (1992); *364*, 316 (1993); *Macromolecules, 26*, 5698 (1993).

[9] H. W. Gibson and P. T. Engen, *New J. Chem., 17*, 723 (1993).

[10] Y. X. Shen, D. Xie, and H. W. Gibson, *J. Am. Chem. Soc., 116*, 537 (1994).

[11] M. Irie, *Adv. Polym. Sci., 94*, 27 (1990).

[12] D. Feng, L. N. Venkateshwaran, G. L. Wilkes, C. M. Leir, and J. E. Stark, *J. Appl. Polym. Sci., 37*, 1549 (1989).

[13] L. N. Venkateshwaran, G. L. Wilkes, C. M. Leir, and J. E. Stark, *Ibid., 43*, 951 (1991).

[14] T. Hashimoto, S. Kohjiya, S. Yamashita, and M. Irie, *J. Polym. Sci., Polym. Chem. Ed., 29*, 651 (1991).

[15] D. Feng, G. L. Wilkes, B. Lee, and J. E. McGrath, *Polymer, 33*(3), 526 (1992).

[16] Y. X. Shen, M. C. Bheda, and H. W. Gibson, *Macromolecules*, Manuscript in Preparation.

[17] D. A. Meyer, in *Vulcanization of Elastomers* (G. Alliger and I. J. Sjothun, Eds.), Reinhold, New York, 1964.

[18] D. Feng, G. L. Wilkes, C. M. Leir, and J. E. Stark, *J. Macromol. Sci.—Chem., A26*(8), 1151 (1989).

[19] S. Abouzahr, Dissertation, Virginia Polytechnic Institute and State University, 1983, p. 152.

[20] Y. S. Ding, S. R. Hubbard, K. O. Hodgson, R. A. Register, and S. L. Cooper, *Macromolecules, 21*, 1698 (1988).

Received February 23, 1994